4.2.3.5 Planetary geology

ERNST HAUBER AND ROLAND WAGNER

4.2.3.5.1 Craters and chronology

Impact craters on solid surfaces of planets and their moons are created by hypervelocity collisions with smaller bodies ranging in size from micrometeorites to large bolides up to tens or hundreds of kilometers in diameter [e.g. 80Pik, 89Mel]. Candidate impactors or projectiles include [e.g. 75Wet, 94Neu, 05Str]:

1. asteroids,
2. comets,
3. remnant bodies of planetary accretion.

Basically, the number or frequency of craters on a given portion of a (solid) planetary surface, such as a geologic unit with a specific origin, records the age of the unit: the higher the crater frequency, the higher the age of the surface due to the longer exposition time towards the incoming projectile flux [e.g. 60Oep, 64Bal, 66Har, 75Neu].

The size-frequency distribution of impact craters is assumed to be correlated with the size-frequency distribution of the projectile family which created the craters [94Neu, and ref.'s therein]. Crater scaling laws describe the relationship between projectile size and impact condition parameters, e.g. impact velocity, impact angle, density of impactors, and surface parameters, such as surface gravity, density and strength of surface materials. Several crater scaling laws are discussed in the literature [e.g. 85Cro, 87Hol, 87Sch, 89Mel].

Crater morphologies reflect physical properties of specific planetary surfaces and changes of these properties with time [e.g. 04Sch].

Cratering chronology models

The crater frequency measured on a specific geologic unit is representative of the relative age or crater retention age of the unit in comparison with other units [79Arv]. Two methods exist to obtain the absolute age of a geologic unit from its crater frequency:

Method 1: Calibration of crater retention ages using radiometric ages of rock samples collected on a specific geologic unit [e.g. 81Har, 94Neu].

Method 2: Calibration of the crater retention ages using known crater formation rates [e.g. 81Har].

Absolute ages obtained with an impact chronology model are generally termed cratering model ages. They are given in units of Giga-years (Gyr or Ga; 1 Ga = 1 billion years) or Mega-years (Myr or Ma; 1 Ma = 1 million years).

Cratering chronology models for the terrestrial planets

The Earth's moon is the only body (except Earth) for which Method 1 is applicable today by using radiometric ages of rock and soil samples from the Apollo and Luna missions (see Section 4.2.6) [e.g. 81Har, 87Wil, 94Neu, 01Neu1].

The lunar impact cratering chronology model is characterized by an exponentially declining impact and crater formation rate in the first ~ 800 million years subsequent to planetary formation 4.55 Ga ago [75Wet, 94Neu]. This period was termed Late Heavy Bombardment (LHB) [75Wet]. Since about 3.8 Ga ago, impact and cratering rates have dropped considerably and reached a more or less constant level at 3 - 3.3 Ga ago [e.g. 75Wet, 94Neu, 01Neu1].

Several groups of authors interpreted a peak in radiometric ages of lunar rocks at about 3.9 Ga as indication for a strong peak in impact and cratering rate around this time [74Ter, 90Ryd, 00Har2]. Based on this interpretation it was concluded that the Late Heavy Bombardment was characterized by a terminal

lunar cataclysm rather than by a smooth, exponential decay in impact rate with time. The lunar cataclysm theory has been challenged by dynamic, geologic and stratigraphic arguments [e.g. 75Wet, 94Neu, 06Bal] but is still debated in the literature [e.g. 06Hie].

For the terrestrial planets in the Inner Solar System, Mercury, Venus and Mars, surface ages can only be obtained by models of the crater forming rates on each one of these bodies (Method 2). Shapes of crater size-frequency distributions measured on the terrestrial planets, including the Moon, were shown to be more or less similar which indicates (a) the same family of bodies, preferentially asteroids (Main Belt, Near Earth asteroids, etc.) impacting these planets, and (b) that time dependences of impact and cratering rates are similar to that for the Moon [e.g. 94Neu, 01Neu1, 05Str].

Lunar-like cratering chronology models were derived for Mercury [88Str, 01Neu2], Venus [97Mck], and Mars [76Neu, 81Neu, 01Har] (see Table 1). On the comparably young surface of Venus (less than an average of 1 Ga), all record of an intense bombardment prior to 3 Ga is lost due to internal activities, and the record of small craters is reduced due to Venus' dense atmosphere causing the destruction of projectiles smaller than a given size [97Mck]. Measurements of crater frequencies were also carried out and surface ages were derived for several asteroids of the Main Belt (MBA) and of the Near Earth Asteroid (NEA) population (e.g. 951 Gaspra [94Neu, 96Cha2]; 243 Ida [94Neu, 96Cha1]; 253 Mathilde [98Cha]; 433 Eros [00Cha]).

Surface ages of the terrestrial planets

A stratigraphic scheme for each terrestrial planet was established, based on stratigraphic key horizons which are defined by geologic criteria and by their superimposed crater frequencies, e.g. crater ejecta, lava materials etc. [e.g. 87Wil, 90Wil, 01Tan]. The geologic history of each planet was subdivided into time-stratigraphic systems. Where necessary, these systems were further subdivided into several (e.g. lower, middle or upper) series.

Time-stratigraphic systems and series correspond to periods and epochs as chronologic criteria [87Wil, 90Wil]. The beginning of each period or epoch and its duration is defined by the cratering model age derived from the crater frequency measurement on the key horizon which defines the base of each system or series [87Wil, 90Wil, 01Tan].

The geologic history of Mercury is subdivided into the following periods (systems), characterized by major impact events, which are from youngest to oldest: Kuiperian, Mansurian, Calorian, Tolstojan, and pre-Tolstojan [88Spu]. The cratering model ages for the stratigraphic key horizons which formed at the beginning of each period are listed in Table 1.

The periods (systems) in the geologic history of Venus, defined by plains formation, tectonic and impact events, are (from youngest to oldest): Aurelian, Guineverian, Fortunian, and pre-Fortunian [98Bas]. Because there is no unique average estimate of the surface age of Venus, absolute ages are preferentially given in fractions of an average surface age T [e.g. 97Mck, 98Bas].

The most extended data set concerning stratigraphy and surface ages is available from the surface of the Moon [87Wil, and ref.'s therein]. The lunar geologic history is subdivided by impact events into the chronologic periods Copernican, Eratosthenian, Imbrian, Nectarian, and pre-Nectarian (corresponding to time-stratigraphic systems with the same names). The Imbrian period is further subdivided by the Orientale impact into a late (upper) and early (lower) Imbrian chronologic epoch (stratigraphic series) [87Wil]. The cratering model ages for the stratigraphic key horizons are listed in Table 1.

The subdivision of the geologic history of Mars is based on key horizons created by plains-forming volcanism [86Tan]. The periods/systems from youngest to oldest are Amazonian (with a late, middle, and early epoch), Hesperian (late and early epoch), and Noachian (late, middle, and early epoch). The Noachian is characterized by the oldest, densely cratered units. Its base is not exposed [86Tan]. The most up-to-date chronology model is by Hartmann and Neukum [01Har]. The cratering model ages of its key horizons are listed in Tab. 1.

Cratering chronologies for the satellites in the Outer Solar System

Two sets of impact chronology models, based on possible crater forming rates, exist for the satellites in the Outer Solar System: (a) models with a lunar-like time dependence of the impact and cratering rate, and (b) models with a constant impact and cratering rate throughout most of solar system history.

Table 1. Chronologic periods and epochs, corresponding to time-stratigraphic systems and series, of the geological histories of Mercury, Moon and Mars. Venus is not included because absolute age data are not widely used for this planet [98Bas]. In columns 2 to 4, the cratering model ages of the stratigraphic key horizons for each period/system are listed. Model ages are given in units of Ga (see text for explanation). No age uncertainties are included for the model ages (see references given in the table for details). Differences in absolute age dating for each planet between various groups of investigators are due to differences in assumptions of the impact and cratering rates. For Mars, for example, the two authors [01Har] came up with either younger ages (Hartmann) or higher ages (Neukum) for the epochs of the Amazonian period but agree for the epochs of the Hesperian and Noachian periods.

Planet / Period (Epoch)	References (1) / Cratering model age	References (2) / Cratering model age	References (3) Cratering model age
Mercury	[88Str]	[01Neu2]	---
Kuiperian	1.0	1.0	
Mansurian	3.0 - 3.5	3.0 - 3.5	
Calorian	3.92	3.77	
Tolstojan	4.1	3.97	
Pre-Tolstojan	> 4.1	> 3.97	
Moon	[87Wil]	[94Neu, 01Neu1]	[01Stf]
Copernican	1.1	1.5	1.1 – 2.1
Eratosthenian	3.2	3.2	3.15
Late Imbrian	3.8	3.84	3.72
Early Imbrian	3.84	3.92	3.77
Nectarian	3.92	4.1	3.92
Pre-Nectarian	> 3.92	> 4.1	> 3.92
Mars	[01Har] (Hartmann)	[01Har] (Neukum)	---
Late Amazonian	0.3	0.66	
Middle Amazonian	1.5	2.47	
Early Amazonian	2.9	3.31	
Late Hesperian	3.65	3.65	
Early Hesperian	3.74	3.74	
Late Noachian	3.86	3.86	
Middle Noachian	3.97	3.97	
Early Noachian	> 3.97	>3.97	

Lunar-like cratering chronology models for the Jovian and Saturnian satellites were derived by several groups of investigators [82Sho1, 85Boy, 85Neu, 85Ple, 97Neu, 98Neu, 06Neu]. One group of authors assumes preferentially comets as major impactors [82Sho1, 85Boy, 85Ple], another group preferentially asteroids from the Main Belt [98Neu, 06Neu].

A constant cratering rate chronology for the icy satellites of the major planets was put forward, based on present-day numbers, sizes, orbital parameters and impact rates preferentially of comets originating in the Kuiper Belt, and extrapolating these impact rates and their uncertainties (factors of 3 - 5) back in time [96Sho, 98Zah, 03Zah, and ref.'s therein].

The two competing cratering chronology models agree well for old, densely cratered surfaces on the icy satellites but are more than an order of magnitude divergent for younger, volcanically and/or tectonically resurfaced units. A discussion of the pro's and con's for each one of these models is beyond the scope of this summary. For this, the authors refer the reader to a series of publications on this issue [e.g. 97Neu, 98Neu, 98Zah, 03Zah, 04Sch].

Surface ages of the icy satellites

The low frequency of craters superimposed on the surface of Europa infers a much younger surface age than for the densely cratered surfaces of Ganymede and Callisto [79Smi2, 82Luc]. The average age of Europa could be 30 - 70 Ma in the comet impact chronology model [03Zah].

With the asteroidal lunar-like chronology model, much higher surface ages on the order of 1 Ga (range from 1.5 to 0.5 Ga due to model uncertainty) are obtained for Europa, but individual geologic units can also be as young as ~ 200 Ma or less [98Neu]. A possible present-day endogenic activity of Europa is not refuted by this model.

The dark, densely cratered plains on Callisto and Ganymede are mostly old in both chronology models, on the order of 4 Ga and older [98Neu, 98Zah, 03Zah]. Major disagreements between the two models exist for the tectonically resurfaced bright grooved terrain on Ganymede (see Section 4.2.3.5.3). Depending on the two cratering chronology models, bright grooved terrain was formed between 3.9 and 3.6 Ga ago [97Neu, 98Neu], ~2 Ga ago [03Zah], or only a few hundred million years ago [98Zah].

Based on lunar-like impact chronology models, the ages of the densely cratered surfaces of the icy satellites of Saturn were estimated to be on the order of 3.8 - 4 Ga old while resurfaced terrains, e.g. on Enceladus and Dione, may have formed less than 1.5 Ga ago [85Boy, 85Ple, 85Neu, 06Neu]. Currently, the large data volume of images returned by the cameras aboard the Cassini Orbiter around Saturn is used to update existing model chronologies [03Zah, 06Neu]. The cometary, constant-rate bombardment history model [03Zah] implies very young ages for the resurfaced terrains on e.g. Enceladus (order of << 1 Ga) but still high ages (> 4 Ga) for the densely cratered units on each satellite [08Kir]. Cassini Radar data show only a small number of large impact craters on Titan implying a very young surface age [06Sto].

Ages of the surfaces of the five major Uranian satellites Miranda, Ariel, Umbriel, Titania and Oberon were obtained by crater counts on Voyager imaging data [87Ple, 88Ple, 89Ple]. Except for Miranda and Ariel, the spatial resolution is low. The densely cratered plains on these satellites are mostly old (order of 4 Ga [03Zah]). Titania shows younger resurfaced terrain with ages of 2 - 3 Ga [03Zah]. The tectonically and/or cryovolcanically resurfaced units on Ariel and Miranda could be much younger, possibly only several 100 Ma [03Zah].

Several groups have worked on crater distributions on Neptun's largest satellite Triton and concluded that its surface could be not older than several Ma up to 600 Ma [03Zah, and ref.'s therein].

Crater morphologies on the terrestrial planets

Impact craters are ubiquitious landforms on the rocky surfaces of the terrestrial planets Mercury, Venus, the Earth's moon, and Mars [e.g. 89Mel]. Main Belt (MBA) and Near Earth Asteroids (NEA) imaged so far also show densely cratered surfaces [94Neu, 96Cha1, 96Cha2, 98Cha, 00Cha]. Earth hosts an average number of 150 confirmed impact features plus a number of less likely cases (order of 50). Most of the terrestrial cratering record has been erased by active geologic processes.

With increasing diameter, crater morphology becomes increasingly complex. Several classes of crater forms can be distinguished [83Pik, 88Pik, 89Mel]. Transitional diameters between these classes depend on the specific physical properties of each body, such as e.g. surface gravity and strength, and therefore vary from planet to planet. Morphologic classes and transition diameters for each planet are listed in Table 2. Typical examples for each morphologic class are shown in Fig. 1. In addition to these morphologic classes, individual craters of each class are subject to erosion, degradation or other (e.g. tectonic) processes and can, in addition, be subdivided by their degradational state (see Section 4.2.3.5.4).

The smallest craters which can be identified in camera images are the so-called simple craters [83Pik, 88Pik, 89Mel]. In their pristine state, simple craters exhibit (a) a sharp crater rim, (b) a bowl-shaped, more or less parabolic crater interior, and (c) a well-developed ejecta blanket. A typical example is shown in Fig. 1 (top left)). At small sizes, crater morphology is preferentially controlled by the strength of the surface material [87Hol, 87Sch].

At diameters larger than a few kilometers, crater forms become complex. The simple-to-complex transition diameter is inversely proportional to the surface gravity [80Pik, 87Hol, 89Mel]. Mars deviates from this rule because of a significant amount of volatiles in the subsurface [80Pik, 89Mel]. Characteristics of this complex crater class are (a) wall terraces, (b) flat floors, and (c) central peaks or peak complexes [89Mel] (example: Tycho, Moon, 85 km, Fig. 1 (middle left)). A further criterion is the depth-to-diameter (d/D) ratio which is significantly smaller than for that of simple craters [see e.g. 80Pik].

At still larger crater sizes, central peak rings can be observed, especially in craters on the Moon or Mercury (example: Fig. 1 (top right); Table 2).

The largest complex craters have diameters of several hundreds of kilometers. Impact structures in this size range are generally termed impact basins [89Mel, 93Spu] (Table 2). These features are characteristic of the oldest geologic units on the terrestrial planets and provide a record of massive impacts in the early geologic history (prior to ~3.7 Ga).

Double-ring craters are small impact basins or so-called protobasins and display large, central peak rings [83Pik, 88Pik] (example: Fig. 1 (middle right); Table 2). With increasing basin diameter, more than two rings can be discerned, formed as concentric ridges or inward-facing scarps [89Mel, 93Spu]. A maximum of six concentric rings in one basin (e.g. Orientale, Moon) was reported [93Spu]. The largest ring basin known on the terrestrial planets is South Pole Aitken (SPA) on the Moon with a maximum diameter of 2600 km of the outermost ring [93Spu].

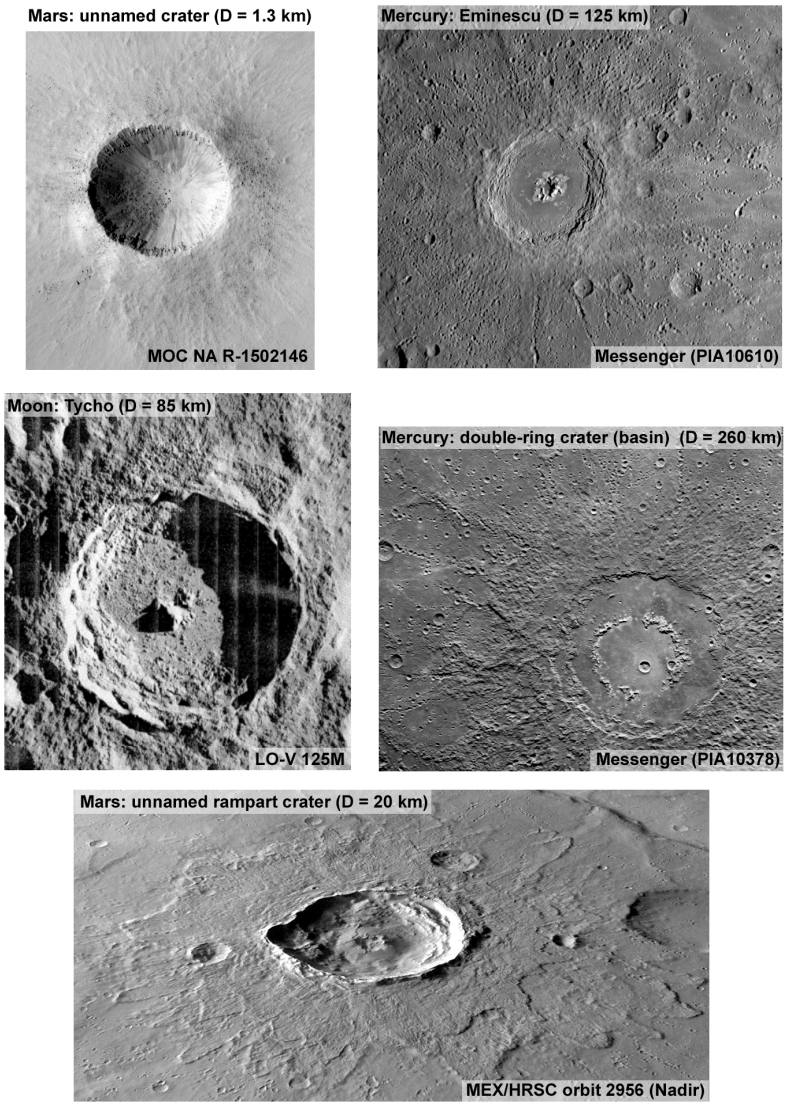

Fig. 1 Type examples of characteristic crater morphology classes on the terrestrial planets (image numbers given at the bottom of each image).
Top left: small simple crater (unnamed) on Mars (MOC narrow angle camera (NA)); middle left: complex crater Tycho with terraces and central peak on the Moon (Lunar Orbiter V); top right and middle right: complex crater Eminescu with central peak ring, and large, complex double-ring crater or basin (unnamed) on Mercury, both images by Messenger MDIS narrow angle camera (flyby Jan. 2008; PIA numbers are from http://photojournal.jpl.nasa.gov); bottom: rampart crater (unnamed) on Mars, data from the HRSC camera aboard MarsExpress, nadir channel frame from orbit 2956.

Ejecta material

The material ejected during crater formation produces two distinct facies of deposits on the surface [e.g. 89Mel]: material ejected over larger distances produces clusters or radial chains of small, more or less irregularly shaped small craters termed secondary craters. This facies is called discontinuous ejecta. Closer to the rim of the crater, a more or less continuous ejecta blanket can be distinguished. Both ejecta facies can be seen in the two Mercurian craters in Fig. 1 (top and middle right). Ejecta are not found on low-gravity bodies, such as asteroids or the two Martian moons [e.g. 94Neu].

Mars exhibits a specific type of continuous ejecta. Their morphology indicates mobilization (fluidization) of volatiles (e.g. H_2O) in the target material, aided by the presence of an atmosphere [89Mel, 06Car, and ref.'s therein]. This class of Martian craters is termed rampart craters. The continuous ejecta show a lobate-shaped outer boundary, in many cases with a terminal ridge (example: Fig. 1 (bottom)).

Crater rays are common for stratigraphically young craters on the Moon and Mercury. Rays are bright, filament-like albedo features which extend several hundreds of kilometers radially outward from the crater [89Mel]. Typical examples are Copernicus or Tycho on the Moon. Crater rays are at best seen in images taken at high sun elevation. Rays fade with time and may have disappeared after 1 - 2 Ga [89Mel]. Their origin is still not fully understood [see discussion in 89Mel].

Table 2. Transition diameters of crater morphology classes for the terrestrial planets. All diameters are given in kilometers. For the simple-to-complex (average) transition diameter [83Pik, 88Pik], min./max. ranges are given in smaller characters. Data for Martian rampart craters (third column) by [06Car], Data for two-ring basins (fourth col.) by [83Pik], for multi-ring basins (fifth col.) by [88Pik] and [93Spu]. Transition diameters for craters and basins on Venus were not exactly measured but have been shown to be more or less similar to craters on Earth [93Spu].

Planet	Simple-to-complex tr.	Rampart cr.	Two-ring b.	Multi-ring b.
Mercury	10 (9 - 30)	-	> 75	> 285
Earth (& Venus)	3.5 (2 - 5)	-	> 25 (?)	> 21
Moon	18 (15 - 25)	-	> 140	> 300
Mars	6.5 (5 - 8)	> 3	> 45	> 300

Crater morphologies on the satellites of Jupiter

The craters on the three Galilean satellites of Jupiter, Callisto, Ganymede and Europa, formed on predominantly icy surfaces. Three trends in crater morphology on these bodies were noted [04Sch, and ref.'s therein]: (1) With increasing diameter, the complexity of crater forms increases, similar to craters on the rocky terrestrial planets. (2) With increasing diameter, crater forms increasingly deviate from crater forms on the terrestrial bodies, with morphologies not observed on e.g. the Moon or Mars at larger sizes. (3) Also unlike craters on rocky bodies, the depth-to-diameter ratio first increases with increasing crater diameter, but decreases after having reached a maximum at a certain diameter specific to each satellite.

No impact craters have been observed on Io because of the high resurfacing rates on this volcanically active body [04McE, and ref.'s therein]. Ganymede and Callisto exhibit large expanses of dark, densely cratered plains implying high surface ages [04Moo2, 04Pap]. On the comparably young surface of Europa, a total number of 150 catalogued (and partly named) craters larger than 1 km and up to 45 km in diameter was reported using Galileo SSI (including Voyager) data [98Moo, 01Moo, 04Sch].

Broadly, five different classes of impact structures can be distinguished on the three icy Galilean satellites [79Smi1, 79Smi2, 82Pas, 04Sch]:

1. classic crater forms – simple and complex craters,
2. craters with central pits,
3. craters with central domes,
4. bright, flat, pancake-shaped forms termed palimpsests,
5. multi-ring structures.

Specific crater forms unknown from terrestrial-planet surfaces are shown in Fig. 2. Transition diameters for the characteristic crater morphologies on the three major icy satellites of Jupiter are listed in Table 3.

Simple craters on the icy Galilean satellites are similar in morphology to their terrestrial-planet analogues [04Sch]. The simple-to-complex transition begins at smaller diameters than on the terrestrial planets [04Sch]. Stratigraphically young complex craters larger than ~ 15 - 20 km can exhibit bright ray systems. Examples for small complex craters are shown in Fig. 2 (top left).

In some complex craters on all three satellites, an outward-facing scarp is observed in the continuous ejecta blanket about one crater radius away from the rim. Complex craters with this specific feature were termed pedestal craters [82Hor, 98Moo, 01Moo, 04Sch]. This feature is reminescent of rampart craters and, as on Mars, infers the presence of volatiles in the subsurface [82Hor]. Fig. 2 shows two typical examples of pedestal craters (Gula and Achelous on Ganymede).

Prior to the Voyager flybys and in the Voyager era (1979 - 1989), viscous relaxation was invoked as the landmark process to cause flat crater forms (including palimpsests described below) on the icy Galilean satellites with time, owing to the rapid viscous creep of the low-strength material on these surfaces [73Joh, 79Smi1, 79Smi2, 82Pas]. Alternatively, relaxation by enhanced rim and floor collaps in this low-strength material is discussed as the dominant process to create flattened crater topography [04Sch, and ref.'s therein].

At larger crater sizes, rimmed central pits replace central peaks in craters on the three icy Galilean moons (Table 3). With increasing diameter, central domes within rimmed central pits are observed in craters on Ganymede and Callisto which are unique on these two satellites [82Pas, 88Moo, 04Sch]. Pit-to-crater and dome-to-crater ratio increases with increasing crater diameter [04Sch]. A typical dome crater is Melkart on Ganymede (Fig. 2).

A fraction of dome craters on Ganymede and Callisto exhibit a comparably large central dome, surrounded by a wreath of rugged terrain instead of a rimmed pit while a prominent, coherent crater rim can no longer be observed. The terminology for such forms is not uniform, they are termed anomalous dome craters [04Sch, and ref.'s therein], large dome craters [88Moo], anomalous pit craters [83Cro], or penepalimpsests type II [82Pas]. A typical example is Neith on Ganymede (Fig. 2).

The origin of central domes is an open issue. The following modes of origin are in discussion: (1) refreezing of impact melt [83Cro], (2) post-impact diapirism [88Moo], or (3) rapid uplift of ductile material during impact [93Sch].

Bright, mostly circular high-albedo impact structures occur on Ganymede and Callisto. First observed in Voyager data, they were interpreted as remnants of former impact craters and termed palimpsests [79Smi1, 79Smi2, 82Pas]. These impact crater forms are almost completely devoid of typical crater morphologies such as crater rims. Palimpsests showing distinctive remnants of concentric structures were classified as penepalimpsests type [82Pas]. A typical example, Buto Facula, is shown in Fig. 2.

The origin of palimpsests (including penepalimpsests) is not fully understood. The following modes of emplacement are discussed [03Jon, and ref.'s therein]: (1) extrusion, triggered by impact, (2) fluidized ejecta, or (3) dry and solid ejecta.

Multi-ring structures are the largest impact features on Callisto and Ganymede with a maximum spatial extension up to several thousands of kilometers. Typical ring structures are Valhalla and Asgard on Callisto, with maximum diameters of their entire ring systems of ~ 3800 km (Valhalla) and ~ 1900 km (Asgard) [79Smi1, 79Smi2, 82Pas, 04Moo2].

Unlike ring structures on the terrestrial planets, these two best preserved ring basins on Callisto are characterized by distinct structural zones with (a) central bright plains reminescent of a palimpsest and up to several hundreds of kilometers in diameter, surrounded (b) by numerous (> 5) concentric rings of ridges, scarps, or troughs with a more or less constant spacing [95Sch, 00Gre1].

On Ganymede, multi-ring structures are also abundant but circularity and structural zones have been altered or obliterated by tectonic deformation [82Pas, 98Pro, 04Pap, 04Sch]. A second type of ring structures on Ganymede like the Gilgamesh basin is characterized by (a) similar structural zones but with a smaller number of rings (< 5), (b) is much less degraded, and (c) shows a smaller frequency of superimposed impact craters, therefore represents relatively young impact structures [04Sch].

On Europa, multi-ring structures, first identified as brown spots in Voyager images [82Luc], are one order of magnitude smaller in diameter than on Ganymede or Callisto. Only two of such forms, Callanish and Tyre, are known [82Luc, 98Moo]. The existence of pits and chains of small craters radial to the center of both features seen in Galileo SSI data represent secondary crater clusters and confirm that Callanish and Tyre have an impact origin [01Moo].

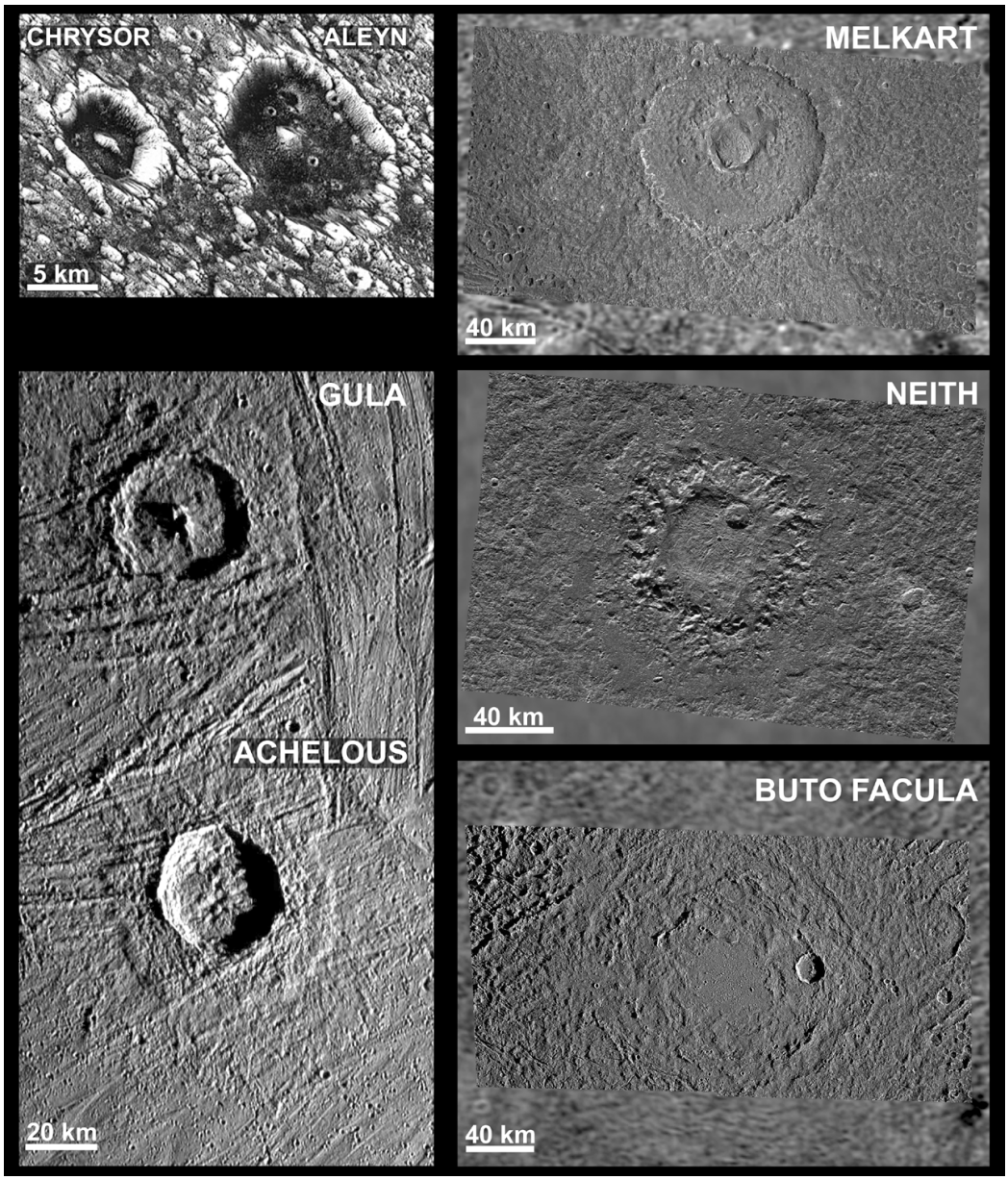

Fig. 2. Typical examples of characteristic crater forms on Ganymede. These craters are also representative of analogous crater forms on Callisto. Image sources: mosaics of Galileo SSI images obtained during various flybys in the Nominal Mission, SSI target area observation ID of each frame is given. Chrysor and Aleyn: small complex craters, target area G1GSMEMPHI01; Gula and Achelous: mid-sized complex craters with ejecta pedestals, target area G7GSACHELS01; Melkart: large central pit crater, target area G8GSMELKRT01; Neith: anomalous dome crater or penepalimpsest, target area G7GSNEITH_01; Buto Facula: palimpsest in dark material of Marius Regio, target area G8GSBUTOFC01. Mosaics in right column shown in lower-resolution Voyager context. North is approximately pointing to the right for Neith and upward for all other images.

Several models describe the origin of multi-ring structures on planets and satellites [89Mel, 93Spu], but only the Tsunami and the ring tectonic models seem to sufficiently explain the specific morphology of these structures on icy satellites. In the Tsunami model [68Van, 93Spu], a massive impact can fluidize the target material and produce wave-like features which are topographically expressed as numerous ridges, scarps, and troughs.

The ring tectonic model [80Mck] describes the origin of rings on icy satellites by a massive projectile which impacts into a thin (order of several kilometers to a few tens of kilometers), brittle lithosphere and penetrates into a ductile, possibly in parts fluid astenosphere. In this model, the material in the astenosphere flows gravitationally inward toward the center of the impact which extensional stresses in the material of the lithosphere.

From width and spacing of troughs or furrows, the brittle-to-ductile transition depths can be measured [80Mck]. On Ganymede and Callisto, this transition was, accordingly, at depths at approximately 15 to 20 km at the time of formation of these basins. On Europa, Callanish and Tyre formed when the brittle-to-ductile transition was at depths of about 5 - 10 km [01Moo].

A special crater form abundant on Callisto are crater chains (catenae) which can reach lengths up to 620 km (Gipul Catena) [82Pas, 95Sch]. Only a small number of such chains are radial to ring basins and therefore secondary crater chains [00Gre1]. The majority of these chains was created by cometary bodies fragmented into a string of bolides hitting the surface, in a process similar to the break-up of comet Shoemaker/Levy-9 which impacted Jupiter in July 1994 [95Mck1, 00Gre1].

Table 3. Transition diameters and diameter ranges for crater morphology classes on the three icy Galilean satellites of Jupiter. Data from Greeley et al. and Schenk et al. [04Gre, 04Sch, and ref.'s therein]. Diameters are given in kilometers. Abbreviations used in the top row are: S2C: simple-to-complex crater transition; CP: central pit craters; CD: central dome craters; PP: penepalimpsest (= craters with a large central dome); P: palimpsests; MRB: multi-ring basins. The smallest palimpsest (~ 50 km) on Ganymede was observed in Galileo SSI data of the first Ganymede flyby [98Pro].

Satellite	S2C	CP	CD	PP	P	MRB
Europa	~ 5 (3 - 27)	--	--	--	--	> 40
Ganymede & Callisto	~ 3 (2 - 35)	> 26	> 60	50 - 250	~ 50 - 390	> 100

Crater morphologies on the satellites of Saturn

The morphology of craters on the nine major icy Saturnian satellites Mimas, Enceladus, Tethys, Dione, Rhea, Titan, Hyperion, Iapetus and Phoebe varies from smaller, bowl-shaped simple craters to complex craters similar to the morphology of craters on the Jovian satellites. Complex craters are characterized by central peaks or peak complexes but lack central pits and domes [86Cha]. Simple-to-complex transition diameters are listed in Table 4.

Craters with bright rays as observed for the Galilean satellites are not commonplace on the satellites of Saturn, only at small crater sizes (a few kilometers and less in diameter) [86Cha, 05Por1, 06Wag, 08Sch]. Among several possible causes cited [e.g. 86Cha], these are low surface gravity and high ejection velocity. One large (48 km in diameter), stratigraphically young ray crater was found on Rhea and is an impact possibly a few hundreds of millions or less than ten million years old, dependent of the crater chronology model [07Wag3, 08Wag].

Cassini ISS data have extended the image data base for large craters, basins and ring structures on the icy satellites of Saturn. The largest number of such structures was found on Iapetus using digital terrain models derived from Cassini ISS stereo data [08Gie]. The largest one of these structures is up to 800 km across [07Gie2, 08Gie].

Rhea's old, densely cratered surface also shows several large impact structures. Tirawa and a degraded basin of similar size adjacent to it to the east were known prior to Cassini [01Sto, 04Moo1, and ref.'s therein]. Most of the large impact structures recently discovered in Cassini ISS stereo images are heavily degraded and therefore difficult to discern [07Gie2, 07Wag3, 08Wag].

The 350-km basin Evander (named recently [08Roa2]) located near the south pole of Dione is the largest impact structure on this satellite. The existence of this basin was anticipated from Voyager imagery [02Sto]. The largest basin on Tethys is Odysseus (445 km in diameter) and a few more mostly degraded basins < 300 km in diameter [02Sto, 04Moo1]. The surface of Mimas is characterized by the 110-km large impact structure Herschel [04Moo1, and ref.'s therein].

Table 4. Average transition diameter, indicated by the occurrence of central peaks, and diameter range for the simple-to-complex crater transition on each of the major satellites of Saturn [86Cha, 89Sce]. Diameters are given in kilometers.

Satellite	Simple-to-complex transition	
Mimas	27.5	(20 - 35)
Enceladus	15	(10 - 20)
Tethys	27.5	(20 - 35)
Dione	20	(15 - 25)
Rhea	15	(10 - 20)
Iapetus	< 49	

The large impact structures are characterized by only one or two rings, mostly ridges or inward-facing scarps [e.g. 04Moo1]. Central peaks or peak complexes can occur in these structures. Differences in topographic expressions of impact structures on various satellites are believed to have been caused by differences in thermal histories of each of these bodies [07Gie2, 08Gie].

Crater morphologies of the satellites of Uranus

Detailed analysis of crater morphologies on the five major Uranian satellites, Miranda, Ariel, Umbriel, Titania and Oberon is hampered by the comparably low image resolution obtained during the Voyager 2 flyby in January 1986, except for Miranda and Ariel [86Smi, 89Sce].

The largest number of simple craters is seen on the surface of Miranda which was imaged at highest spatial resolution [86Smi, 91Cro]. Complex craters on all five major Uranian satellites are characterized by central peaks [89Sce] (Table 5). Central pits, domes, or palimpsests are absent in complex craters [91Cro]. An 11-km high mountain seen on the limb of Oberon could represent an enormous central peak of a large impact basin [86Smi, 91Cro].

Table 5. Average transition diameter or diameter ranges, indicated by the occurrence of central peaks, for the simple-to-complex crater transition on each of the major satellites of Uranus [86Cha, 89Sce]. Diameters are given in kilometers. Limited image coverage and resolution does not allow to better constrain the simple-to-complex transition diameter and diameter ranges for central peaks [89Sce].

Satellite	Simple-to-complex transition
Miranda	> 25
Ariel	15 (10 - 20)
Umbriel	< 29
Titania	< 20
Oberon	< 35

Ariel, Titania and Oberon exhibit craters with bright rims, bright ejecta and rays [86Smi]. Umbriel lacks craters with bright ejecta or rays, except for a single bright annular feature 40 km in diameter of unknown origin [86Smi]. Large, basin-type impact structures > 100 km in diameter occur on the surfaces of Umbriel, Titania and Oberon [86Smi, 91Cro].

Crater morphologies on the satellites of Neptune

Neptune's largest satellite Triton exhibits very low crater frequencies implying young surface ages [89Smi, 03Zah]. Simple craters are observed to a maximum diameter of 12 km [89Smi]. Larger craters show the typical complex morphology with flat floors and central peaks, but central pits, domes or palimpsests do not occur on Triton. The largest crater found on Triton's surface has a diameter of 27 km [89Smi].

4.2.3.5.2 Volcanism

Volcanism has shaped the surfaces of all terrestrial planets and the Moon, and still occurs on the Jovian satellite, Io (Fig. 3 and Fig. 4). Other moons of Jupiter and Saturn display evidence for cryovolcanism, and active eruptions have been observed on Enceladus, a small icy moon of Saturn. Volcanic landforms result from internal processes that transport heat from a planet`s interior outwards, and the study of past and present volcanic activity can put important constraints on the internal evolution of a geologic body (Ref. section 4.2.3.4.: Dynamics and Thermal Evolution). The investigation of the morphology and mineralogy of volcanic products as well as the study of eruption processes allows to infer the composition of parent magmas derived from the crust or mantle and, indirectly, to the chemical composition of planetary interiors. Therefore, an understanding of the volcanic history of a geologic body is of paramount importance.

This chapter gives an overview of the most important volcanic landforms in the Solar System. It is not intended to give a comprehensive summary of all volcanic surface features and processes, since there are many excellent reviews available (general volcanology: [72Mac, 79Wil, 88Cas, 04Fra, 00Sch1, 00Sig]; basaltic volcanism: [81BVS]; planetary volcanism: [89Cat, 96Mur, 96Fra, 99Wil, 00Zim2, 83Wil]). Since this chapter is about surface geology, it discusses extrusive volcanism only, and does not treat impact melts (according to the IUGS, impact melt rocks are crystalline, semihyaline or hyaline rocks which have solidified from shock-produced impact melt).

Eruptive processes and environmental control

Any specific planetary environment influences the eruption conditions of volcanic processes. The atmospheric conditions (if an atmosphere is present), the particular surface gravity, and the density profile within the lithosphere all affect the ascent and eruption of magma as well as the cooling of lava flows and other volcanic deposits. An analysis of these parameters and their role in volcanic processes is provided by [83Wil, 84Wil1]. These different environmental parameters have to be kept in mind during any attempt to relate observed volcanic deposits to eruption mechanisms (Table 6).

Fig. 3. Huge basaltic volcanic constructs on the larger terrestrial planets. **(a)** Maat Mons on Venus, a steep-sided volcano that rises three kilometers above the surrounding terrain. Lava flows extend for hundreds of kilometers across the fractured plains shown in the foreground, to the base of Maat Mons. The simulated perspective view was created on the basis of Magellan radar data and color images of the Venera 13 and 14 landers (image: NASA/JPL). **(b)** Huge terrestrial shield volcanoes such as those found on the Galapagos or Hawaiian Islands are often used as analogues for the giant Martian shield volcanoes. The image shows the snow-covered caldera of Mauna Loa on Hawaii (Mauna Kea in background). Note the similarity to the caldera of the Martian shield volcano, Olympus Mons, displayed in panel c (image: USGS/D.W. Peterson). **(c)** The summit region of Olympus Mons with its large, 80 km-diameter caldera. This and other images proved immediately and beyond doubt that volcanoes exist on Mars (image: NASA).

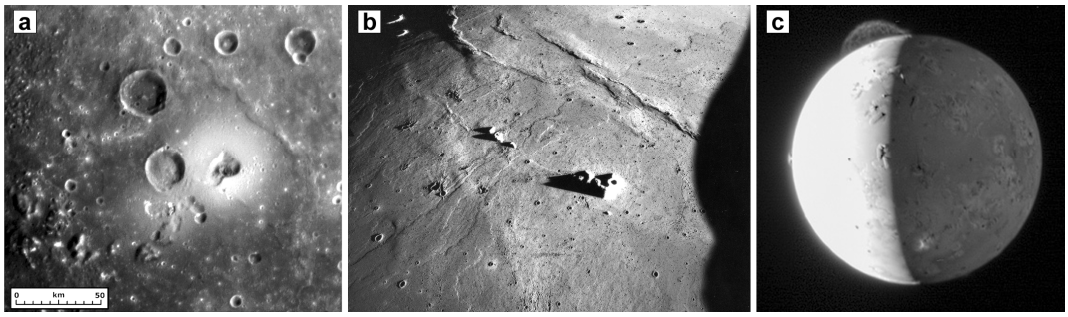

Fig. 4. Evidence for volcanism on smaller Solar System bodies. **(a)** Dome-like feature with central, kidney-shaped depression on Mercury. This object was recently discovered by the MESSENGER spacecraft and is interpreted as a broad and low shield volcano [08Hea], similar to lunar domes. Image: NASA/Johns Hopkins University Applied Physics Laboratory/Carnegie Institution of Washington. **(b)** Lava flows on the lunar surface bear testimony that volcanism was a significant process on the Moon (image: Apollo 15, M-1556). **(c)** The plume of Tvashtar volcano spectacularly rises over the surface of the Jovian satellite, Io, against the dark background of space [07Spe]. Another smaller plume, associated with the volcano Prometheus, is visible on the left. Tvashtar`s plume reaches a height of 290 km (terrestrial volcanoes erupt their gas and dust just a few kilometers high). The image was taken on 28 February, 2008, by the New Horizon spacecraft on its way to Pluto during an encounter with the Jovian system (image: NASA).

Table 6. Types of volcanc eruptions (after [99Wil]).

Type of eruption	Characteristics [99Wil]
Effusive eruptions	Magma erupts from a vent without significant disruption and forms a lava flow
Explosive eruptions	Magma is disrupted into fragments (pyroclasts) by expansion of exsolved gases
Strombolian	Eruptions in which large, pressurized bubbles of volcanic gas emerge intermittently from a vent and burst, disrupting the magma surface into a spray of pyroclasts
Vulcanian	Intermittent explosive eruptions in which gas pressure builds up beneath a retaining cover of cooled lava until the strength of this layer is exceeded
Hawaiian	Steady discharge of volcanic gas and incandescent pyroclasts forms a (fire) fountain above the vent
Plinian	Vigorous explosive eruption in which a relatively steady discharge of volcanic gas and hot pyroclasts entrains and heats gas from the surrounding atmosphere to form a high convecting eruption cloud above the vent
Phreato-magmatic	Explosive eruption involving the vigorous interaction of erupting magma with surface water or any other liquid volatile
Pyroclastic eruption into a vacuum	No atmosphere, no convecting eruption cloud (e.g., Moon, Io)

The factors controlling magma ascent of the Moon have been examined by, e.g., [81Wil]. Of particular interest is Mars, because it has an atmosphere that is dense enough to support convection clouds, but thin enough to enable explosive eruptions. Explosive basaltic eruptions should be common on Mars, because the combination of lower gravity and low atmospheric pressure favours the nucleation of gas bubbles and fragmentation of magma in greater depths than on Earth [82Fra, 94Wil]. A modern

theoretical treatment of tephra production and dispersion on Mars is given by [07Wil1], and the heat transfer in volcano-ice interactions on Earth [07Wil2] and some implications for Mars are analyzed by [02Wil2, 07Hea1]. Venus, on the other hand, has a extremely dense atmosphere, which will tend to suppress explosive eruptions [86Hea]. Water contents of Venusian magmas would have to be much higher than on Earth to enable explosive eruptions, and it is likely that explosive activity might have never happened on Venus (Tab. 7). Effusion rates on other planets and moons can not be measured in situ, and have to be derived from morphometric data (Tab. 8).

Table 7. Surface pressures on planets and minimum water content of magmas to enable explosive eruptions (from [99Wil]).

Planet	Surface atmospheric pressure [MPa]	Minimum water content [weight-%]
Earth	0.1 (land)	0.07
	60 (ocean floor)	
Mars	0.00005 - 0.0005 (depending on elevation)	0.01
Venus	4 - 10 (depending on elevation)	2
Moon, Io	0	-

Table 8. Rheologic properties of lava flows and effusion rates on Earth, Moon, Venus, Mars, and Io (modified from [07Hie]; b.: basalt, tr.-and.: trachyte/andesite, carbon.: carbonatite, phonol.: phonolite).

Location	Yield strength [Pa]	Viscosity [Pa s]	Effusion rate [$m^3\ s^{-1}$]	Lava type	Ref.
		Earth			
Makaopuhi, Hawaii	10^2			basalt	68Sha
Mauna Loa, Hawaii	3.5×10^2 - 7.2×10^3	1.4×10^2 - 5.6×10^6	417 - 556	basalt	87Moo
Columbia Riv. Basalts	$< 7 \times 10^3$			basalt	84McB
Makaopuhi, Hawaii	70 - 8×10^3	7×10^2 - 4.5×10^3		basalt	84Cig
Makaopuhi, Hawaii	4×10^3 - 2×10^4				78Moo
Mount Etna, Italy	10^3 - 5×10^4			basalt	85Kil
Mount Etna, Italy			0.3 - 0.5	basalt	76Pin
Kilauea, Hawaii	1.5×10^3 - 5×10^4			basalt	86Fin
Mauna Loa, Hawaii	0.4×10^4			basalt	78Moo
Hawaii	0.23 - 1.1×10^4			trachyte	78Moo
Mount St. Helens	1.5×105			andesite	78Moo
Mono Craters (USA)	1.2 - 3.3×10^5			rhyolite	78Moo
Sabancaya, Peru	4.99×10^4 - 1.57×10^6	7.26×10^9 - 1.64×10^{13}	1 - 13	tr.-and.	03War
Oldoinyo Lengai, Tanz.		10 - 100		carbon.	90Daw
Columbia Riv. Basalts		5.0 - 4×10^3		basalt	73Mur
Mauna Loa, Hawaii		1.7×10^5		basalt	76Hul
Paricutin, Mexico		3.6×10^6		andesite	76Hul
Arenal, Costa Rica		1.0×10^7		b.-and.	84Cig
Arenal, Costa Rica			0.33	andesite	84Pin
Teide, Tenerife		4.4×10^7		phonol.	76Hul
Kilauea, Hawaii			2 - 400	basalt	90Row
Mauna Loa, Hawaii			5 - 1044	basalt	90Row
Laki (Iceland)			8700 (max)	basalt	93Tho

Location	Yield strength [Pa]	Viscosity [Pa s]	Effusion rate [$m^3 s^{-1}$]	Lava type	Ref.
Moon					
Mare Imbrium	1.5×10^2				75Moo
Mare Imbrium	4.2×10^2				77Hul
Mare Imbrium	2×10^2				73Boo
Gruithuisen Domes	$7.7 - 14.2 \times 10^4$	$3.2 - 13.9 \times 10^8$	5.5 - 119.3		03Wil
Mairan Domes	$5.3 - 13.1 \times 10^4$	$1.3 - 11.5 \times 10^8$	48.0 - 51.5		03Wil
Aristarchus	1.3×10^4				77Hul
Aristarchus	1.94×10^4				78Moo
Necho	2.25×10^4				78Moo
King	2.41×10^4				78Moo
Venus					
Artemis Festoon Lobe 1	4.12×10^4	7.12×10^6	1.02×10^4		04McC
Ovda Festoon Plains	2.07×10^5	9.28×10^9	2.4×10^2		04McC
Atalanta Festoon	1.22×10^5	2.34×10^9	9.52×10^2		04McC
Artemis Festoon Lobe 2	1.32×10^5	7.31×10^9	2.54×10^3		04McC
Mars					
Arsia Mons	$0.39 - 3.1 \times 10^3$				78Moo
Arsia Mons	$2.5 \times 10^3 - 3.9 \times 10^3$	9.7×10^5	$5.6 \times 10^3 - 4.3 \times 10^4$	b./b.-and.	03War
Alba Patera	$1.9 \times 10^3 - 2.8 \times 10^4$	$1.7 \times 10^5 - 1.9 \times 10^6$			87Cat
Ascraeus Mons	$3.3 \times 10^3 - 8.3 \times 10^4$	$6.4 \times 10^5 - 2.1 \times 10^8$	18 - 60		85Zim
Olympus Mons	$8.8 \times 10^3 - 4.5 \times 10^4$	$2.3 \times 10^5 - 6.9 \times 10^6$			76Hul
Olympus Mons	$1.8 - 5.3 \times 10^4$				78Moo
Elysium Mons			20		95Kes
Alba Patera			10^5		97Sak
Ascraeus Mons	$2.0 \times 10^2 - 1.3 \times 10^5$	$1.7 \times 10^4 - 4.2 \times 10^7$	23 - 404		07Hie
Io					
	Outburst (January 1990)		$10^5 - 10^6$	95Bla, 96Dav	
	Open channel flow (Pillan)		$10^3 - 10^4$	01Dav, 01Wil1	
	Lava lake (Pele)		~250 to 350	01Dav, 86Car	
	Amirani (insulated flow field)		79 (+9, –6)	00Dav	
			16 - 245	Equation 3 [03Dav]	
			58	Equation 4 [03Dav]	
	Prometheus (insulated flow field)		35 (+8, –3)	00Dav	
			6 - 88	Equation 3 [03Dav]	
			21	Equation 4 [03Dav]	
	All 14 G1 volcanoes		16 - 55	00Dav	
			3 - 277	Equation 3 [03Dav]	
			9 to 65	Equation 4 [03Dav]	

Volcanic landforms

Volcanism results in a wide range of surface morphologies, basically all of which have also been observed on other planets and moons. Central eruptions create some of the most spectacular of volcanic landforms, i.e. central volcanoes. They can be monogenetic (i.e., formed during one eruption period [79Woo]), or polygenetic (formed during several eruption periods). Central volcanoes can be classified into several types: Shield volcanoes, domes, cinder cones, composite volcanoes, craters, and calderas. If magma interacts with groundwater or seawater, the eruption is called a phreatic eruption, which can result in maars, tuff cones, and tuff rings. Subglacial eruptions (e.g., in Iceland or Antarctica) give rise to characteristical, steep-sided and flat-topped table mountains (called tuyas). Diatremes result from explosive eruptions and the infilling of the vent with breccia. Fissure eruptions are typical for the mid-ocean ridges on Earth, but are also common on the continents, where they feed the lava flows forming the

vast flood basalt provinces. Pyroclastic deposits can form different deposits. Convecting Plinian eruption clouds with heights of up to 50 km can create wide-spread airfall deposits (ash). If an eruption cloud collapses, a pyroclastic flow (a mixture of hot, incandescent pyroclasts, gas, and entrained air) can form and travel at high speeds (>100 m s^{-1}) for large distances (tens of kilometers). The resulting volcanic deposit is an ignimbrite (also called ash-flow tuffs), a mixture of pumice and ash, which can be welded or unwelded. If a volcanic dome collapses, nuées ardentes can create block-and-ash flows, made up from lava blocks with fine vesicles.

Moon

Besides Earth, the Moon is probably the most intensively explored body in the Solar System. Volcanism on the Moon has been the subject of numerous studies dating back to the pre-Apollo era. Today it is known that the majority of volcanic terrains on the Moon are associated with the dark mare regions (or pl. maria). Only minor volcanic features like some apparently volcanic domes and light plains of possible volcanic origin were found outside the maria. Overviews of lunar volcanic processes and landforms are given by, e.g., [76Hea], [76Sch], [87Wil], and [06Hie]. Useful general sources for geologic information about the Moon are the "Lunar Source Book" book edited by [91Hei] and a recent collection of reviews edited by [06Jola]. Technical accounts on lunar exploration, containing a wealth of information on missions and instruments, are available from [99Har] and [07Sto]. An Earth-based (telescopic) perspective is given by [03Woo].

Magma composition

The smooth surfaces and obviously level contacts of the mare materials with the surrounding highlands led to early speculations that a liquid or liquid-like material filled ancient topographic depressions, and although alternative hypotheses were published (e.g., pyroclastic flows [69Mac]), many researchers agreed early on that the nature of this material was basaltic in origin [e.g.,63Bal]. Samples of the mare materials were returned to terrestrial laboratories by the Apollo missions and found to be basalts throughout [81BVS], and thus the term mare materials can be considered to be synonymous to basalts (Table 9) (see [87Wil] and references therein). Viscosities of lunar lavas are not uniform. Based on the morphometry and spectrophotometry of lunar mare domes, [03Wil] and later [07Woe] and [07Len] concluded that the viscosity of the lavas building the lunar mare domes is variable and ranges from 10^2 Pa s - 10^4 Pa s for very flat (0.5° - 2°) domes in Mare Tranquillitatis, to 10^6 Pa s - 10^8 Pa s for the relatively steep (~1.5° - 5.5°) domes near Hortensius [07Woe]. The even steeper (up to 15°) Gruithuisen and Mairan highland domes were built by lavas with viscosities as high as 10^9 Pa s [03Wil, 07Woe]. For comparison, lunar mare lavas have viscosities on the order of ~1 Pa s [70Mur, 71Wei].

Volcanic landforms

Volcanic landforms on the Moon show a smaller degree of variability than terrestrial basaltic landforms. Most notably, no large shield volcanoes with caldera structures were found. Instead, the mare regions are characterized by lava flows (Fig. 4b) that form very level surfaces. Vent structures are rarely observed, and typically the lava flows can not be traced back to their sources. When basalt samples were molten in laboratories, they were found to have very low viscosities [91Hoe], which explains why lunar mare lavas can obviously flow over very long distances (flow lengths of 1200 km [73Sch]) and typically do not show steep flow fronts [71Hol, 76Gre]. A particular type of landform associated with mare volcanism are sinuous rilles, meandering channels that often start at a circular or elongate depression and gradually disappear into the lava plains of the maria [71Gre2]. The lengths can range from a few kilometers to more than 300 km [70Sch]. There is a consensus among many researchers that the channels are formed by a combination of mechanical and thermal erosion of the underlying substrate [e.g., 73Hul, 04Wil].

The total area covered by basaltic lavas is about 17% of the lunar surface or 7×10^6 km^2 [76Hea]. If cryptomaria are included, this number increases to ~20%. Cryptomaria are mare regions that have been covered by other materials, mostly impact ejecta. Most mare lavas are contained in near-side basins. Estimates on the thickness of lavas [e.g., 76DeH, 79DeH, 78Hoe, 98Bud] yield maximum thicknesses of ~1 - 2 km and a total volume of 6×10^6 km^3 [75Hea, 78Thu]. A review of the techniques applied to determine mare basalt thicknesses is given by [82Hea]. The volumes of individual basalt flow units can vary substantially, but are, on average, between ~590 km^3 and ~940 km^3. Although there is considerable

uncertainty involved in these values, it is clear that mare basalts are volumetrically minor (~1% of the volume of the lunar crust; [76Hea]) and that there was no large-scale partial melting involving significant parts of the mantle. Other volcanic landforms of the mare regions include volcanic mare domes, e.g., in the Marius Hills, [76Gue, 80Hea], lava terraces [71Hol], and cinder cones [76Gue]. Summaries of volcanic landforms of mare regions are given by [76Sch] and [78Mas].

Table 9. Major element concentrations (in weight-%) in representative lunar mare basalts (after [**91Tay**].

	Reference	SiO_2	Al_2O_3	FeO	MgO	CaO	K_2O	TiO_2	Cr_2O_3	MnO	Na_2O
High-Ti											
Apollo 11 High-K 10049	81BVS	41.0	9.5	18.7	7.03	11.0	0.36	11.3	0.32	0.25	0.51
Apollo 11 Low-K 10003	81BVS	39.8	10.4	19.8	6.7	11.1	0.06	10.5	0.25	0.30	0.40
Apollo 17 70215	81BVS	37.8	8.8	19.7	8.4	10.7	0.05	13.0	0.41	0.27	0.36
Apollo 17 Orange Gl. 74220	81BVS	38.6	6.3	22.0	14.4	7.7	0.09	8.8	0.75	–	0.36
Low-Ti											
Apollo 12 Pigeonite 12064	81BVS	46.3	10.7	19.9	6.5	11.8	0.07	4.0	0.37	0.27	0.28
Apollo 12 Olivine 12002	81BVS	43.6	7.9	21.7	14.9	8.3	0.05	2.6	0.96	0.28	0.23
Apollo 12 Ilmenite 12051	81BVS	45.3	10.0	20.2	7.0	11.4	0.06	4.7	0.31	0.28	0.29
Apollo 15 Pigeonite 15597	81BVS	48.0	9.4	20.2	8.7	10.4	0.06	1.8	0.48	0.30	0.32
Apollo 15 Olivine 15545	81BVS	45.2	8.6	22.1	10.3	9.8	0.04	2.4	0.68	0.30	0.31
Low-Ti, aluminous											
Luna 16 21013,8	79Ma	-	13.3	19.1	6.0	11.7	0.21	5.1	0.20	0.26	0.55
Apollo 14 14321 Gp. 5	85Dic	-	11.8	17.5	10.3	10.8	0.01	2.6	0.46	0.24	0.39
Apollo 14 14053	81BVS	46.4	13.6	16.8	8.5	11.2	0.10	2.6	-	0.26	-
Apollo 14 14321 Gp. 1	85Dic	-	12.7	16.2	7.9	11.2	0.16	2.2	0.37	0.22	0.60
Apollo 14 VHK 14305,390	85She	-	13.0	16.0	9.9	11.6	0.80	2.2	0.59	0.20	0.41
Very-Low-Ti											
Apollo 17 70007,296	79Wen	-	10.3	17.0	12.0	9.7	0.01	0.4	0.64	0.26	0.15
Apollo 17 78526	79Wen	-	11.0	17.5	11.0	9.9	0.02	0.9	0.83	0.27	0.15
Luna 24 24174,7	78Lau	46.0	12.1	22.1	6.0	11.6	0.02	1.1	0.30	0.28	0.26
Luna 24 24109,78	78Ma	-	11.6	22.4	7.0	12.3	0.02	1.3	0.38	0.26	0.29
Apollo 15 Green Gl. 15426	81BVS	44.1	7.8	21.0	16.7	8.4	0.03	0.37	0.33	-	0.13

Several areas on the Moon display an unusually high concentration of volcanic features [71Gue, 76Gue], e.g., the Marius Hills or the Aristarchus Plateau /Rima Prinz region [77Whi]. These areas might have been the source areas for multiple eruptions with high effusion rates and large volumes. Regional dark mantle deposits, mostly associated with uplands adjacent to younger mare regions, are interpreted to be pyroclastic materials. [81Wil, 83Wil] find that Hawaiian-style fire fountaining, driven by continuous gas exsolution, dispersed pyroclastic material over tens to hundreds of kilometers. Pyroclastic glass formed by lava foutaining of gas-rich, low viscosity and Ti-Fe-rich basaltic magmas [74Hei] is volumetrically negligible but scientifically important, insofar as it is derived from melts generally unaffected by crystal fractionation and represents the best samples of the lunar mantle [06Hie]. Reviews of the lunar basalt types are given by, e.g., [92Nea], [98Pap], and [06Luc].

In comparison to mare basalts, the non-mare volcanic features are relatively insignificant. Most notably, some obviously volcanic domes can reach diameters of 20 km and heights of >1000 m. Prominent examples are the Gruithuisen domes, whose shape suggests that they consist of viscous lava, and the Mairan domes, which might be explosive in nature. More ambiguous is the interpretation of light plains as volcanic materials, because an origin as impact breccias (as suggested by returned samples) or other processes can not be ruled out.

Chronology of volcanism

The ages of mare basalts have been determined by radiometric dating of samples [e.g., 01Nyq] and by crater statistics [e.g., 00Hie, 02Hie, 03Hie]. A detailed overview of lunar chronology is provided by [06Stf]. Mare volcanism appears to have lasted at least from before ~4.0 Ga to perhaps as late as ~1.2 Ga, but work by [83Sch] suggests that volcanism might have started even earlier and may have lasted even longer than this. The intensity of volcanism was not uniform throughout this time span. Crater counts indicate that volcanism peaked at about 3.5 Ga and drastically declined after that time [00Hie, 02Hie, 03Hie]. Averaged effusion rates seem to be very low, even during the peak period of activity, and have been estimated at $\sim 10^{-2}$ km^3 a^{-1} (comparable to those at individual terrestrial volcanoes like Hawaii) [92Hea1] (Table 10). Individual eruptions, however, were probably associated with very high effusion rates, separated by long periods of inactivity [e.g., 91Hea2].

Table 10 Magma volumes on planetary bodies (values from [**91Gre**]).

Planet-ary body	Mass/ Earth mass	Total extrusives [10^6 km^3]	Extrusive production [km^3 yr^{-1}]	Total magma production [km^3 yr^{-1}]	Scaled extruded production [km^3 yr^{-1}]	Scaled total production [km^3 yr^{-1}]	Ref.
Venus	0.815		≤ 2.0	≤ 19	≤ 0.082	≤ 0.78	87Gri, 91Hea1
Earth	1.000		3.7 to 4.1	26 to 34	1.0	1.0	84Cri
Moon	0.012	10	0.0024	0.025	0.052	0.069	92Hea1
Mars	0.107	68.8	0.018	0.17	0.042	0.052	91Gre

Magmatism and tectonism

Moon is a one-plate planet with a stagnant lid and does not display evidence for plate tectonics. Instead, lunar tectonism is restricted to contraction due to global cooling and to local effects (e.g., loading due to filling of basins with dense basalt) (see Section 4.2.3.5.3). The magmatism on the Moon, therefore, is not controlled by Earth-like tectonic environments. From the above description of lunar volcanic landforms, another distinct difference between the Moon and the larger terrestrial planets, Earth, Venus, and Mars, becomes apparent: In contrast to these planets, no large shield volcanoes or calderas have been found on the Moon. These features form when shallow neutral buoyancy zones and magma reservoirs are present, and their absence on the Moon suggests that such zones do not exist. This can be explained by the low density of the lunar crust. Petrologic models of lunar magma generation ([70Rin, 75Hub, 76Rin, 81BVS, 82Tay] see also the recent review by [06She]) suggest that magma is generated in depths of 200 - 400 km [92Nea, 99She]. Since the crust is less dense than the diapirs, it acts as a buoyancy (density) trap and prevents their further ascent – the diapirs stall at the base of the crust in significant depths (an additional rheological trap is created by the cooling of the mantle rock through which the diapir rises, and the tickening of the lithosphere). Further ascent of the magma is only possible if the basaltic diapirs are overpressurized and propagating dikes penetrate to the surface. This model [91Hea2, 92Hea1] would explain why basaltic eruptions are more common on the nearside with its thinner crust, but fails to explain why basalts are not common in the large South Pole-Aitken basin. A better knowledge of crustal thickness variations, compositional variations with depth, and global basalt compositions are required to improve eruption models [06Hie].

Mercury

Mercury is the least explored of the terrestrial planets, and its surface is not yet completely covered by images. For several decades, images taken by the Mariner 10 probe in 1974 and 1975 were the only source to study its surface in spatial detail. The available images covered about 45% of the surface, and no huge volcanoes could be observed, such as those discovered on Mars or Venus. Plains units, morphologically similar to lunar volcanic plains, were considered to be the most plausible candidate volcanic landforms [e.g., 75Mur]. However, Mercury does not display composition-related differences in reflectance, which exist on the Moon between the primary anorthositic crust of the highlands and the secondary volcanic crust that is exposed in the mare regions. Since the resolution of the Mariner 10 images was limited (typically 1 km/pixel), no unambiguous morphologic evidence for volcanism, e.g., flow lobes or vent structures, could be identified [78Mal]. This was not so suprising, however, because [02Mil] demonstrated that in images of similarly low resolution of the lunar surface it is also not possible to unambiguously identify volcanic landforms, although they exist. [97Rob] found evidence for Mercurian volcanism in Mariner 9 colour data, and this work was among the most convincing studies in favour of volcanism on Mercury before the first MESSENGER flyby. A collection of review of pre-MESSENGER results is provided in a special issue of the Journal of Geophysical Research [1975], in the Mercury book edited by [89Vil], and by [07Str]. An easily accessible introduction to Hermean science [03Str] also covers Mariner 10 and Earth-based observations, and [08Hei] summarize the preliminary results of the first MESSENGER flyby.

In January 2008, the MESSENGER spacecraft imaged another 21% of the surface that had not be seen before with resolutions as high as 150 m/pixel. The images show strong evidence for volcanic landforms, including irregularly-shaped depressions without raised rims, flooding and embayment of impact craters, floor-fractured craters, and radial graben systems [08Hea]. Perhaps the most unambiguous volcanic landforms are the irregular, “kidney”-shaped depressions. A particularly striking example is located at the southern margin of the Caloris basin (Fig. 4a). The depression is ~20 km long, lacks a raised rim (in contrast to impact craters), and is surrounded by materials with smooth surfaces. Near the depression, a bright material seems to mantle the underlying terrain and becomes diffuse outwards after a radial distance of about 25 km from the depression. This bright material is interpreted by [08Hea] as pyroclastic deposits, whereas the darker smooth terrain surrounding the depression might be (basaltic) lava flows. Topographically, the entire feature might be a domical structure, on the basis of shading effects, buried massifs nearby, and embayment relationships. The closest analogy might be lunar mare domes [80Hea], and the interpretation of the depression and the diffuse bright materials as volcanic vent and pyroclastic deposits, respectively, is partly based on lunar analogues [74Luc]. Other evidence for possible volcanism is shown in Fig. 5.

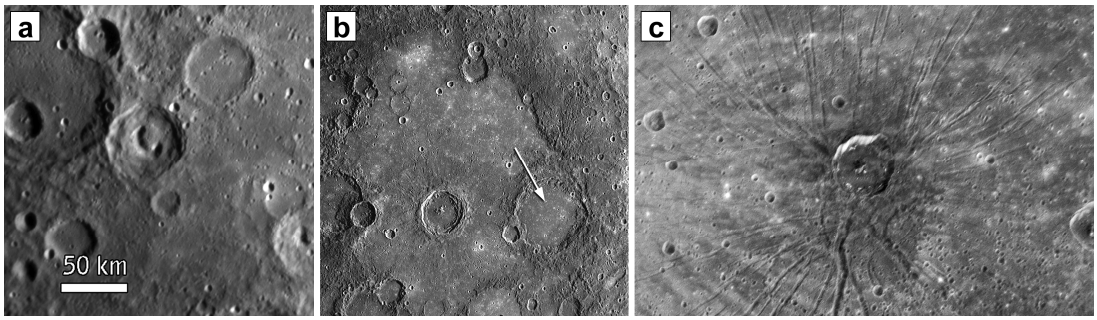

Fig. 5. Examples of possible volcanic features on the surface of Mercury. (a) Telephone-shaped collapse feature on the floor of an unnamed 52 km-diameter crater (illumination from the right). Such a collapse feature could reflect past volcanic activity at and just below the surface of this particular crater. (b) The 120 km-diameter crater Rudaki (arrow) displays a floor of smooth plains, which are far less cratered than the neighboring terrain. Some craters in the plains appear to have been significantly flooded with lava, leaving only their circular rims preserved. (c) Pantheon Fossae, a set of radial grabens inside the Caloris Basin. The origin is unknown, but one interpretation [08Hea] is that the grabens are underlain by volcanic dikes. All images: NASA/Johns Hopkins University Applied Physics Laboratory/Carnegie Institution of Washington.

Mars

A wealth of data from orbiting and landed missions shows that volcanism on Mars is widespread and of diverse nature. In terms of the number and the extent of volcanoes and volcanic surfaces, it is intermediate between the large terrestrial planets, Earth and Venus, on the one hand, and the smaller bodies in the inner Solar System, Mercury and the Moon, on the other hand. Mars has a thin atmosphere and is, again, distinct from Earth and Venus with their thick atmospheres and the small bodies without atmospheres, Mercury and the Moon. Reviews on Martian volcanism are provided by [75Car], [81Gre], [92Mou], [00Zim1], and [00Gre2], and there are chapters on volcanism in the Mars books by [81Car] and [07Car]. An atlas of volcanic landforms on Mars illustrates many examples of basaltic volcanic features [94Hod].

Magma composition

Volcanism on Mars, as on all terrestrial planets, is mainly basaltic (Table 11). This notion was first supported by the inspection of landforms, which show extreme similarities to terrestrial basaltic landforms [e.g., 74Gre], and later by the analysis of SNC meteorites (thought to come from Mars), which yields a basaltic composition [e.g., 94McS, 02McS], and the in situ investigation of images and samples on Mars by landed missions [77Mut, 77Bin, 97Rie, 98Dre, 00Lar, 99McS, 03McS, 04McS]. Moreover, the detection of wide-spread pyroxenes and olivine in spectral data acquired by orbiting spacecrafts indicate mafic compositions of surface materials [05Chr, 05Bib, 07Pou] (Fig. 6). Whether more evolved lavas than basalt were emplaced on the Martian surface is a matter of debate (e.g., orbital spectra might indicate dacitic [05Chr] and quarzo-feldspathic [04Ban] compositions). Two types of spectra in dark (i.e. dust-free) regions have been detected: One interpretation is that this is indicative of the occurrence of two types of volcanic compositions: basaltic and basaltic-andesitic to andesitic [00Ban1]. Alternatively, [02Wya] suggested that the "andesite" of [00Ban1] is actually weathered basalt. A recent review of Martian surface mineralogy is available in [07Che].

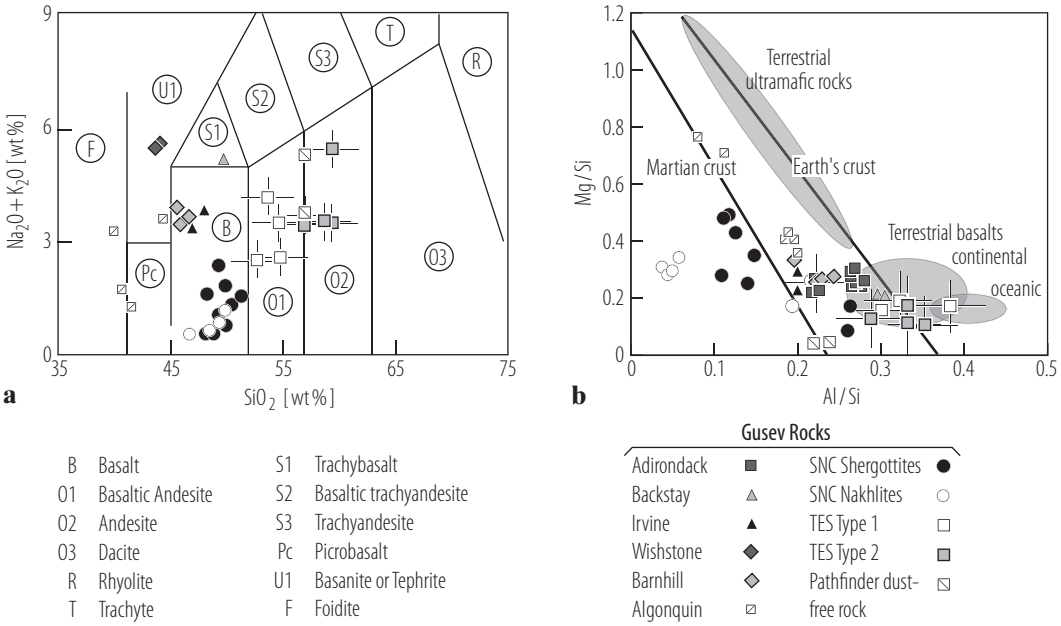

B	Basalt	S1	Trachybasalt
O1	Basaltic Andesite	S2	Basaltic trachyandesite
O2	Andesite	S3	Trachyandesite
O3	Dacite	Pc	Picrobasalt
R	Rhyolite	U1	Basanite or Tephrite
T	Trachyte	F	Foidite

Fig. 6. Composition of Martian volcanic materials. (a) Petrologic classification of volcanic rocks in Gusev Crater, as determined by the MER rover Spirit (modified from [08McS], [04McS]). (b) Mg/Si versus Al/Si variations in rocks in Gusev Crater (modified after [04McS], [01Wae]).